Multiscale Analysis of Turbulence in Horizontal Pipes

Savari, Chiya; Barigou, Mostafa

DOI:
10.1063/5.0193241

Document Version
Publisher's PDF, also known as Version of record

Citation for published version (Harvard):
Savari, C & Barigou, M 2024, 'Multiscale Analysis of Turbulence in Horizontal Pipes: Liquid and Particle-Liquid Flow Investigation', *Physics of Fluids*, vol. 36, no. 3, 033311. https://doi.org/10.1063/5.0193241

RESEARCH ARTICLE | MARCH 05 2024

Multiscale analysis of turbulence in horizontal pipes: Liquid and particle-liquid flow investigation

Special Collection: Overview of Fundamental and Applied Research in Fluid Dynamics in UK

Chiya Savari ; Mostafa Barigou

Physics of Fluids 36, 033311 (2024)
https://doi.org/10.1063/5.0193241

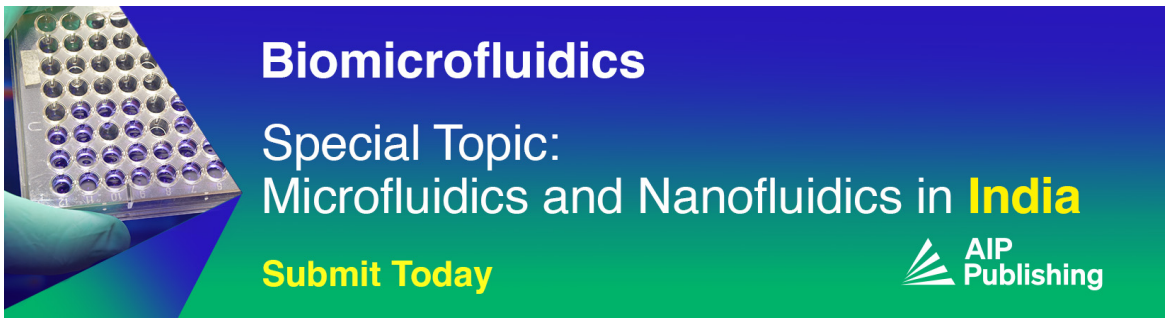

Physics of Fluids ARTICLE pubs.aip.org/aip/pof

Multiscale analysis of turbulence in horizontal pipes: Liquid and particle-liquid flow investigation

Cite as: Phys. Fluids **36**, 033311 (2024); doi: 10.1063/5.0193241
Submitted: 21 December 2023 · Accepted: 9 February 2024 ·
Published Online: 5 March 2024

Chiya Savari and Mostafa Barigou[a)]

AFFILIATIONS

School of Chemical Engineering, University of Birmingham, Edgbaston, Birmingham B15 2TT, United Kingdom

Note: This paper is part of the special topic, Overview of Fundamental and Applied Research in Fluid Dynamics in UK.
[a)]**Author to whom correspondence should be addressed:** m.barigou@bham.ac.uk

ABSTRACT

An experimental–theoretical methodology is developed to investigate the characteristics of turbulence in horizontal particle-liquid pipe flows. Using a discrete wavelet transform, the three-dimensional Lagrangian trajectories of the liquid phase experimentally determined by positron emission particle tracking are decomposed into their deterministic and stochastic sub-trajectories, which are then utilized to construct profiles of local fluctuating velocity components and turbulent kinetic energy. The results for a single-phase flow are independently validated using computational fluid dynamic simulation and the analysis parameters are fine-tuned using direct numerical simulation data from the literature. In a particle-liquid flow, the investigation explores the influence of various factors including particle size, density, and concentration on turbulence intensity. Remarkably, the results demonstrate significant effects of the particle size and density on liquid turbulence. The enhanced understanding gained regarding turbulence intensity helps to advance our fundamental interpretation of the dynamics of particle-liquid flows, thus potentially aiding the rational design of such complex flows and associated equipment.

I. INTRODUCTION

Hydraulic conveying of coarse particles plays a pivotal role in various industries. Understanding and effectively managing these flows are of utmost significance for a spectrum of industries including mining, construction, food and pharmaceutical processing, chemicals, consumer goods, oil, river engineering, and power generation.[1] Efficient design of these flows ensures optimal production rates, minimizes wear and erosion of equipment, maximizes safety, and enhances productivity, cost-effectiveness, and sustainability across a diverse range of sectors. Turbulence often plays a crucial role such that the efficiency and the quality of these flows are determined by the understanding of turbulence characteristics, including parameters such as turbulent kinetic energy (TKE), its magnitude, and spatial distribution. Accessing turbulence properties in pipe flows poses a serious challenge due to the complexities involved in conducting pointwise experimental investigations of internal pipe flows. Insufficient understanding of pipe flow hydrodynamics can result in significant manufacturing issues, leading to substantial financial losses amounting to billions of dollars annually.[2]

TKE is a fundamental parameter that provides insight into the intensity and fluctuations of turbulence within a flow. Various experimental methods have been developed to measure TKE and its dissipation rate, each offering unique advantages and limitations. One commonly used technique is hot-wire anemometry, which utilizes a heated wire to measure the velocity fluctuations caused by turbulence.[3,4] Accurate positioning and alignment of the wire probe are critical, however, for obtaining precise measurements.[5] Although the technique enables direct measurement of TKE and its dissipation rate, it requires multiple hot-wire probes to measure all three-dimensional (3D) velocity components and their gradients, which can introduce substantial disturbances in the flow.[6] Another approach is laser Doppler anemometry (LDA), which employs laser light to measure the velocity of particles within the flow, allowing for the calculation of TKE.[7,8] Similarly, particle image velocimetry (PIV) is another laser-based technique that provides detailed velocity field information for TKE analysis.[7,9,10] Such advanced optical techniques are, however, ineffective in opaque particle-liquid flows since they rely on transparent walls and fluid media. Therefore, TKE measurements by LDA/PIV methods have been restricted to very dilute suspensions in transparent conduits.[7] Positron emission particle tracking (PEPT) is a powerful technique used for tracking and analyzing the motion of individual positron-emitting radiolabeled tracers within complex flow systems.[11]

PEPT provides 3D Lagrangian trajectories, and the velocity field of the flow can be accurately determined from these trajectories. PEPT has proved particularly valuable in studying complex multiphase flow systems where traditional methods face challenges due to opacity, particle size, or complex flow patterns.[12–16]

Pipe flow exhibits a range of turbulence scales, each contributing to the overall complexity and dynamics of the flow. At the largest scales, the flow is characterized by large eddies or vortex structures known as energetic motions.[17] These large-scale structures are responsible for the transport of momentum and energy within the flow. As the flow progresses downstream, these large eddies break down into smaller eddies through a process known as energy cascade.[18] This leads to the development of intermediate-scale eddies that interact with the flow at a more localized level. Finally, at the smallest scales, the turbulent kinetic energy is dissipated through molecular viscosity.[18] These small-scale motions, often referred to as the Kolmogorov scales, are highly chaotic and contribute to the dissipation of energy. Understanding and characterizing these different turbulence scales is crucial for predicting flow behavior, optimizing industrial processes, and designing efficient pipe flow systems.

A comprehensive approach involving both theoretical and experimental methods is essential for assessing flow turbulence properties in a pipe. Precise experimental techniques play a vital role in determining turbulence characteristics, while appropriate theoretical methods are crucial for the analysis of experimental data. The Lagrangian trajectories obtained from PEPT offer a wealth of 3D flow information that can be utilized to deduce a comprehensive understanding of turbulence scales in a pipe. These trajectories encompass both deterministic displacements characterized by low frequencies and stochastic displacements characterized by high frequencies. The deterministic component reflects the bulk or background flow motion, while the stochastic component captures the movement of small-scale fluid parcels. By decomposing the Lagrangian trajectories into their deterministic and stochastic parts, valuable insight can be gained into both the macro- and micro-movement of the flow. Wavelet decomposition, specifically the discrete wavelet transform (DWT), is a powerful signal processing technique that enables simultaneous analysis of signals in both time and frequency domains. It has emerged as a popular method for extracting meaningful information from a wide range of signals, including audio, image, and biomedical data.[19–21] The DWT breaks down a signal into different frequency components using a set of wavelet functions that are localized in both time and frequency. This decomposition provides a multi-resolution representation of the signal, where fine-scale details are captured at higher frequency bands and coarse-scale features are represented at lower frequency bands. By applying the DWT, 3D PEPT trajectory features and structures can be effectively analyzed at different scales, making it a valuable tool in studying turbulence characteristics of pipe flows.

In this study, a multiscale analysis of 3D PEPT Lagrangian trajectories is employed to examine the turbulence properties within a single-phase and particle-liquid pipe flows. The trajectories undergo a discrete wavelet decomposition to separate their deterministic and stochastic components. These decomposed parts are then utilized to construct maps of local mean velocity (background) and fluctuating velocity. The proposed methodology is first validated for a single-phase flow by a Eulerian Reynolds-averaged Navier–Stokes (RANS) computational fluid dynamic (CFD) simulation and by the well-known theoretical one-seventh power law relationship for velocity distribution in turbulent pipe flow. Turbulence intensity data obtained by direct numerical simulation (DNS) available in the literature[22] are then used to fine-tune the main wavelet methodology input parameter, which is the number of decomposition levels required for the analysis. The effects of particle concentration, size, and density on the local TKE profiles are investigated. This approach provides comprehensive insight into the turbulence properties of pipe flows, with the potential to aid the optimum design of particle-liquid transport systems.

II. EXPERIMENT

A. Pipe flow loop

A schematic representation of the experimental flow loop used is depicted in Fig. 1. The flow was driven by a vortex pump (T21-32 HF4 LB1, Turo vortex pump, EGGER, Switzerland) and passed through a

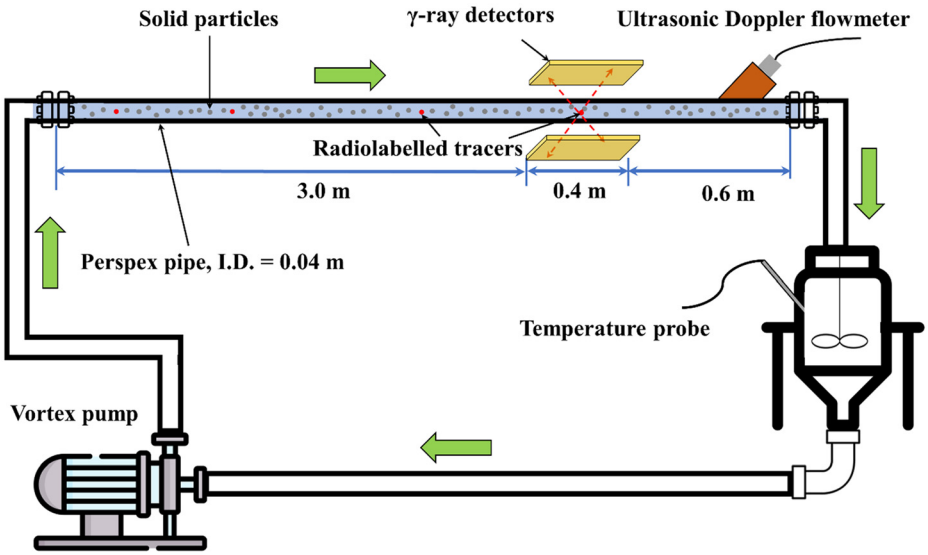

FIG. 1. Experimental pipe flow loop.

Perspex pipe with an internal diameter of 0.04 m. The section used for flow imaging was 0.4 m long and located 3 m downstream of the upstream pipe bend to ensure fully developed flow free from bend effects.[23] The volumetric flow rate of the particle-liquid mixture was measured in real-time using a Doppler ultrasonic flow meter (UF D5500, Doppler flow meter, Micronics). Such measurements were independently verified at the outlet using stopwatch and bucket measurements, which also yielded the average particle delivery concentration. A temperature probe was used to monitor the temperature of the mixture. The carrier fluid used was a 36 wt. % aqueous sugar solution of Newtonian rheology having a density of 1138 kg m^{-3}. The dispersed phase consisted of mono-size nearly spherical calcium alginate particles, produced in-house following the procedure described in Ref. 24. Flow imaging was achieved by the Lagrangian technique of positron emission particle tracking, as described below. Different particle sizes, densities, and concentrations were examined in this study, and the experimental conditions are summarized in Table I. Particle density was controlled by introducing silica powder into the alginate solution during the particle fabrication process.

B. Positron emission particle tracking

PEPT utilizes positron emitting particle tracers as flow followers to track the phases present (liquid, solid) in three-dimensional space and time, enabling precise determination of their long-term 3D Lagrangian trajectories. Unlike other optical visualization techniques, PEPT uniquely allows particle tracking in opaque fluids and inside opaque equipment. Our previous studies have demonstrated that PEPT's accuracy is comparable to that of PIV and LDA.[25] The method has been extensively used to investigate various flow phenomena, and detailed information about the technique, its hardware, and software can be found in our earlier publications.[11,26–30] Here, PEPT measurements were performed using γ-ray detectors providing a 0.4 m field-of-view (Fig. 1). Typically, an appropriate single particle tracer is introduced into a closed flow loop to track a particular flow component. The particle tracer is allowed to circulate until it maps the entire flow area of interest, thus providing a statistically representative number of trajectories (typically > 50). Alternatively, multiple identical tracers are introduced in the flow to help reduce experimental time.

C. Experimental procedure

Prior to any measurements, the suspension was circulated for a duration of 2 h until it reached a steady state. This ensured that the suspension attained a stable temperature and maintained a consistent viscosity (and therefore Reynolds number) throughout the test. During this time, any trapped air was also removed from the flow loop. In all tests, a mean flow velocity of 0.75 m s^{-1} was selected, resulting in a pipe Reynolds number (Re) of 7800. After reaching steady state, the radiolabeled tracers were introduced into the flow loop. In the context of pipe flow, usually 50 trajectories are sufficient to reconstruct the flow.[31] However, in this study, we aimed to enhance data statistics and reduce experimental time by sequentially introducing eight tracers into the flow, resulting in approximately 1500 trajectories in 1 h. The solid and liquid phases were tracked separately. The liquid phase was tracked using 150 μm neutrally buoyant resin particle tracers activated with ^{18}F. For tracking the solid phase, the tiny resin tracers were encapsulated inside representative calcium alginate particles.

TABLE I. Experimental particle-liquid flow conditions.

Particle diameter, d_p (mm)	2, 4, 6
Mean particle concentration, C_s (vol. %)	0, 6, 12, 21, 31
Mean mixture velocity (m s^{-1})	0.75
Pipe Reynolds number, Re (-)	7800
Temperature (°C)	21
Kinematic viscosity, υ (m^2 s^{-1})	3.87×10^{-6}
Liquid density (kg m^{-3})	1138
Particle to fluid density ratio, ρ_r (-)	1.02, 1.14
Resin particle tracer diameter, d_t (μm)	150
Stokes number, St (-)	0.07

For faithful tracking of fluid streamlines by a tracer, equilibrium flow conditions are usually assumed for a Stokes number $St \ll 1$.[32] The Stokes number is defined as the ratio of the characteristic time of the PEPT tracer to a characteristic time of the flow,

$$St = \frac{\tau_p}{\tau_\eta} = \frac{1}{18}\frac{\rho_t}{\rho}\left(\frac{d_t}{\eta}\right)^2, \tag{1}$$

where ρ_t and ρ are the tracer and fluid densities, respectively, d_t is the tracer diameter, and η is the Kolmogorov length scale. In pipe flow, the fluid dissipation rate (ε) and subsequently the Kolmogorov length scale vary radially within the pipe. In this work, St was estimated using the Kolmogorov length scale based on the average value of dissipation rate, i.e., $\eta = (\upsilon^3/\varepsilon)^{1/4}$, where υ is the kinematic viscosity. The average value of the dissipation rate for a single-phase flow was obtained from the CFD simulation for $Re = 7800$, giving $St = 0.07$. Since St is much less than 1, the resin particle tracers could be safely regarded as fluid tracers.

III. DATA HANDLING

A. Local flow component velocity and particle concentration

As PEPT measurements provide 3D Lagrangian space and time data for the different components of the flow, the local instantaneous Lagrangian velocities for each component can be calculated as follows from the local time-derivatives of the respective 3D trajectories:

$$\boldsymbol{u} = u_x\boldsymbol{e}_x + u_y\boldsymbol{e}_y + u_z\boldsymbol{e}_z = \frac{dx}{dt}\boldsymbol{e}_x + \frac{dy}{dt}\boldsymbol{e}_y + \frac{dz}{dt}\boldsymbol{e}_z, \tag{2}$$

where t is time, $\boldsymbol{e}_x$, $\boldsymbol{e}_y$, and $\boldsymbol{e}_z$ are unit vectors, and x, y, z are the Cartesian components of the particle position vector. The local time-derivatives can be estimated through a differencing technique by considering the ratio of distance to time in each direction.

The solid particle distribution in the pipe can also be inferred from the PEPT trajectories. A 3D grid composed of equal volume cells is employed to represent the pipe domain. Traditionally, the occupancy of a tracer in each cell has been defined as the fraction of the total experimental time (t_∞) spent by the tracer in that cell. However, this definition is influenced by the density of the grid, and as the number of cells increases, the occupancy tends to zero.[33] To overcome this subjectivity, the ergodic time (t_E) can be utilized as the time a tracer would spend in a cell assuming the system is single phase and ergodic. In the case of equal volume cells, t_E is defined as the total experimental time divided by the total number of cells, i.e., $t_E = t_\infty/N_c$. The concept

of ergodic time suggests that the tracer has an equal probability of being present anywhere within the pipe. Consequently, the local occupancy (O_E) can be defined as $\Delta t/t_E$, where Δt represents the time spent by the tracer inside a specific cell. Our previous studies[15,33] demonstrated that the local occupancy is equivalent to the ratio of the local solid volume concentration (c) to the mean volume concentration of solids in the pipe (C_s). By employing these definitions, it becomes possible to estimate the local solid phase distribution in the pipe.

B. Multiscale Lagrangian trajectory decomposition

The Lagrangian flow trajectories obtained from PEPT contain valuable information for estimating the average and fluctuating velocities of the flow. A Lagrangian trajectory is comprised of two distinct elements: a low-frequency component that represents the deterministic background portion of the trajectory and a high-frequency component that represents its stochastic part. Mathematically, this can be expressed as

$$\boldsymbol{T}(t_i) = \boldsymbol{T}_{det}(t_i) + \boldsymbol{T}_{sto}(t_i) \rightarrow \begin{cases} x(t_i) = x_{det}(t_i) + x_{sto}(t_i) \\ y(t_i) = y_{det}(t_i) + y_{sto}(t_i) \\ z(t_i) = z_{det}(t_i) + z_{sto}(t_i) \end{cases} \quad i = 1, 2, 3, \ldots, n, \tag{3}$$

where $\boldsymbol{T}$ is the 3D Lagrangian flow trajectory and x, y and z are Cartesian coordinates. The subscripts *det* and *sto* refer to the deterministic and stochastic components, respectively. The variable n represents the total count of position points that form the trajectory.

Wavelet analysis is a powerful decomposition technique used in signal processing and data analysis.[20] It allows for a comprehensive examination of signals at different scales, making it particularly effective for studying transient phenomena. The basic principle behind wavelet analysis involves decomposing a signal into various frequency components, revealing both localized and global information. Thus, by using wavelets, we can decompose 3D Lagrangian flow trajectories and capture both the high-frequency details and the low-frequency trends present in such trajectories simultaneously. The decomposition process involves passing the trajectory components through a series of filters at different scales. These filters extract information within specific frequency ranges, thus facilitating analysis of the trajectory behavior at different resolution scales. The resulting output consists of approximation coefficients, representing the low-frequency components, and detail coefficients, representing the high-frequency components. This hierarchical representation provides a multi-resolution view of the trajectory, enabling features to be discerned at different scales.

As the original 3D PEPT trajectories are discrete, the discrete wavelet transform was accordingly used in this study, which is mathematically defined as follows:

$$DWT(j,f) = \frac{1}{\sqrt{|2^j|}} \int a(t)\psi\left(\frac{t - f.2^j}{2^j}\right) dt, \tag{4}$$

where ψ is the mother wavelet function, $a(t)$ represents a Cartesian coordinate (x, y, or z) signal, and f and j are time lag coefficient and wavelet decomposed information, respectively. DWT uses a discrete set of scales and positions to analyze the signal and provides a discrete-time and multi-resolution representation of the signal. The Mallat algorithm,[34] also known as the Mallat pyramid algorithm, is widely used for implementing the DWT. It provides an efficient and computationally fast approach for decomposing a signal into its approximation and detail coefficients at different scales or decomposition levels. In this algorithm, the original signal is passed through a pair of analysis filters: a low-pass filter and a high-pass filter. These filters capture the low-frequency and high-frequency components of the signal, respectively. Then the signal is convolved with the low-pass and high-pass filters, resulting in two sets of convolved signals, namely, the approximation $A(t)$ and detail $D(t)$ sub-signals. The decomposition process is repeated on the approximation sub-signal obtained in the previous step. This recursive procedure continues until the desired level of decomposition is reached. Thus, the original signal can be completely reconstructed from its decomposed approximation and detail sub-signals as follows:

$$a(t) \approx A_j(t) + D_j(t) + D_{j-1}(t) + \cdots + D_1(t) \quad j = 1, 2, 3, \cdots, L, \tag{5}$$

where L is the number of decomposition levels.

In this multiscale signal decomposition process, we can effectively separate the stochastic fluctuations in the flow tracer trajectory from the overall mean flow motion, enabling us to uncover the turbulent properties of the flow. As illustrated in Fig. 2, the decomposed components of each coordinate can be utilized to reconstruct two distinct Lagrangian sub-trajectories. Specifically, the approximation sub-signals (A_j) are employed to reconstruct the deterministic sub-trajectory, while the detail sub-signals (D_j) are utilized to reconstruct the stochastic sub-trajectory. The deterministic sub-trajectory that shows the mean or background component of the trajectory, as depicted in Fig. 2, closely resembles the original trajectory, but it exhibits a smoother tracer movement that represents the flow motion at the larger scales, specifically advection without the presence of smaller fluctuations. On the other hand, the stochastic sub-trajectory represents the fluctuation components of the original trajectory and captures the smallest scales of the fluid flow, namely, eddy and molecular diffusion. By studying these two sub-trajectories instead of the original trajectory, we can analyze the flow behavior and successfully capture the fluctuations resulting from turbulence within the stochastic sub-trajectory. However, if we were to examine the original 3D trajectory from a single-scale perspective, important flow characteristics such as turbulence properties may be obscured and would be difficult to extract.

C. Turbulent kinetic energy

Turbulent kinetic energy quantifies the energy associated with the chaotic, unpredictable motion of a turbulent flow. It can be defined based on the velocity fluctuations within a turbulent flow, where the fluid velocity exhibits irregular and chaotic fluctuations in multiple directions and at various scales. In the Reynolds-averaged equations, the instantaneous velocity can be separated into its average and fluctuating components,

$$u_i = \overline{u}_i + u_i', \tag{6}$$

where u_i, $\overline{u}_i$, and u_i' are instantaneous, mean, and fluctuating velocity along the i-coordinate, respectively. The velocity fluctuations contribute to the total kinetic energy of the turbulent flow, which is distinct from the kinetic energy associated with the mean flow. If the mean

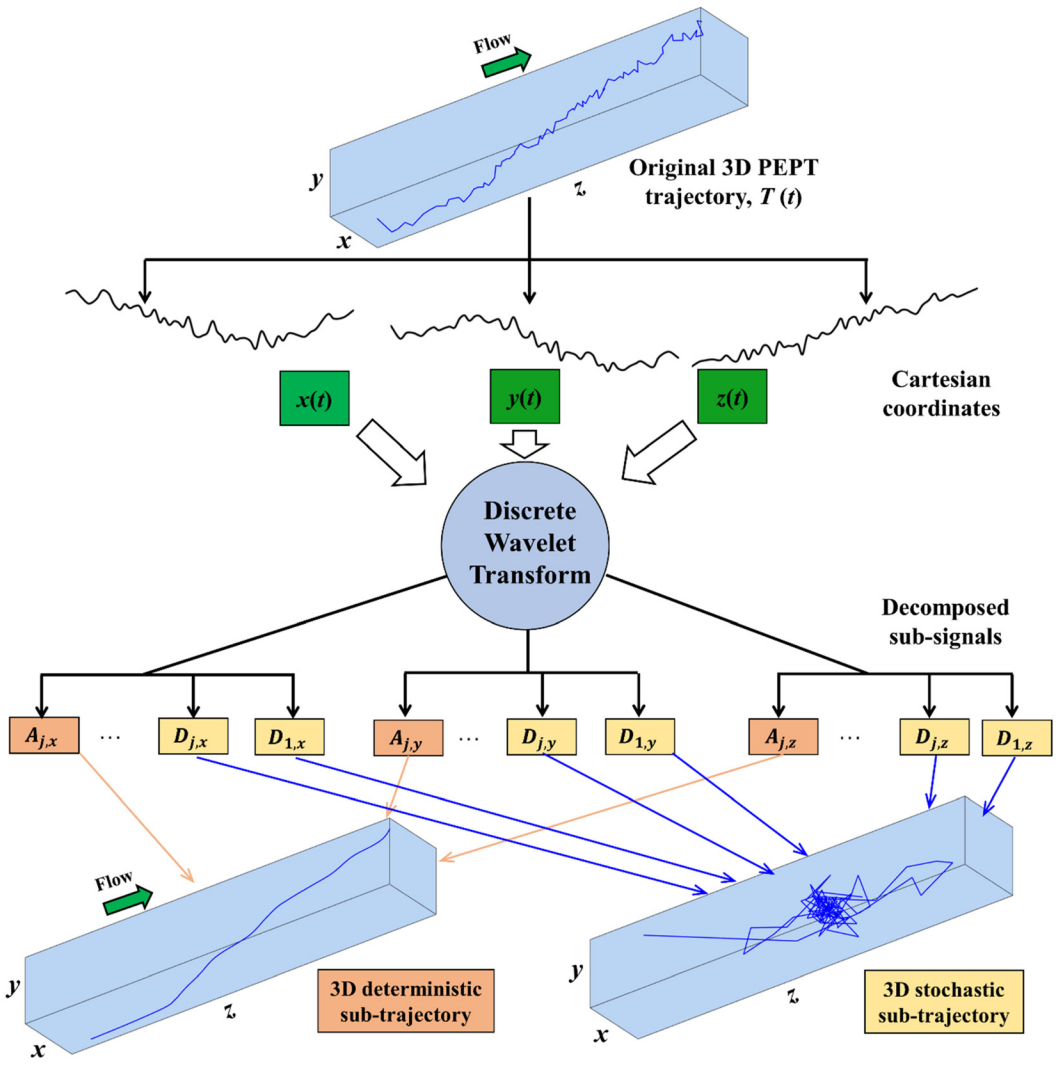

FIG. 2. Flow diagram of wavelet decomposition of a 3D Lagrangian PEPT trajectory.

and instantaneous velocity fields are available, it becomes possible to estimate the fluctuation velocity field and, consequently, the turbulent kinetic energy. Like the Lagrangian instantaneous calculations discussed above, the local Lagrangian mean (background) velocities can be estimated from local time-derivatives of the deterministic 3D sub-trajectory as follows:

$$\overline{\boldsymbol{u}} = \overline{u}_x \boldsymbol{e}_x + \overline{u}_y \boldsymbol{e}_y + \overline{u}_z \boldsymbol{e}_z = \frac{d\overline{x}}{dt}\boldsymbol{e}_x + \frac{d\overline{y}}{dt}\boldsymbol{e}_y + \frac{d\overline{z}}{dt}\boldsymbol{e}_z, \tag{7}$$

where $\overline{x}$, $\overline{y}$, and $\overline{z}$ are Cartesian coordinates of the deterministic sub-trajectory. Thus, a Lagrangian dataset of both instantaneous and mean velocities can be computed. Subsequently, the Lagrangian fluctuation velocities ($\boldsymbol{u}'$) can be obtained from the difference between the instantaneous and mean velocities i.e., $\boldsymbol{u}' = \boldsymbol{u} - \overline{\boldsymbol{u}}$. By obtaining the fluctuation velocities in all three directions, the Lagrangian TKE values (k) can be estimated using the following equation:

$$k = \frac{1}{2}\left(\overline{u_x'^2} + \overline{u_y'^2} + \overline{u_z'^2}\right), \tag{8}$$

where u_x', u_y', and u_z' are, respectively, the fluctuation velocities in the x, y, and z directions.

IV. RESULTS AND DISCUSSION

As discussed above, the local 3D Lagrangian velocities were calculated based on the local time-derivatives of the 3D Lagrangian PEPT trajectories. To construct the Eulerian velocity profiles across the pipe, the Lagrangian data were organized into radial bins and then averaged to analyze the radial distributions of different parameters. The radial bins were designed so that each bin contains the same fraction of the pipe cross-sectional area.

The PEPT velocity measurements were validated for a single-phase (water) flow using a standard RANS Eulerian CFD simulation conducted under the same experimental conditions and by the

well-known theoretical one-seventh power law relationship for velocity distribution in the turbulent pipe flow. To tune the number of decomposition levels in the proposed multiscale wavelet methodology, literature data on the radial distribution of fluctuating velocities obtained from DNS simulations of a single-phase liquid flow were used.[22] Since DNS data are derived from direct numerical solutions of the Navier–Stokes equations free from any modeling assumptions, they can be regarded as a reliable benchmark for validation purposes. After validation and fine-tuning, the wavelet decomposition technique was then used to investigate the turbulence characteristics of the liquid phase in more complex particle-liquid flows over a range of flow conditions.

A. Single-phase flow

1. Mean velocity statistics

The radial profile of the normalized mean axial velocity component (U_z/U_b), estimated from the original PEPT trajectories is depicted in Fig. 3 for half of the horizontal pipe section, alongside the mean axial velocity profiles obtained from CFD and theory at the same pipe Reynolds number ($Re = 7800$). The Eulerian CFD simulation was performed using the Ansys Fluent platform. The governing equations for the simulation were the RANS equations, and the k–ε turbulence model was used. The inlet boundary condition consisted of a uniform velocity profile deduced from the experimentally measured mean flow rate, whereas at the outlet of the pipe, the boundary condition was the local static pressure. The no-slip boundary condition was applied to the pipe wall. The well-known theoretical one-seventh power law $u/u_{max} = (1 - r/R)^{1/7}$, which is a good approximation to velocity distributions in turbulent flow in smooth pipes for $Re < 10^7$,[35] is also plotted in Fig. 3. There is excellent agreement between the PEPT measurements, the CFD, and the theoretical velocity profiles, confirming the high accuracy of PEPT measurements in capturing the characteristics of the turbulent pipe flow. Error bars representing the standard deviations of PEPT velocities in each radial bin are too small to be shown on the plot.

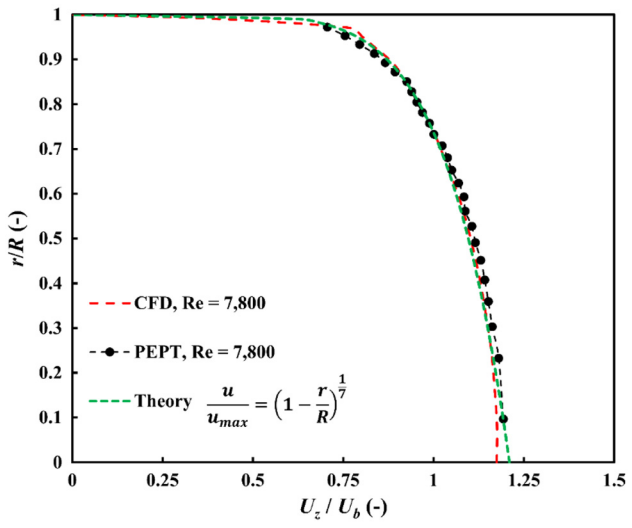

FIG. 3. Normalized mean axial velocity profiles: PEPT, theory, and CFD simulations compared. Error bars of PEPT data points are too small to be shown.

In Fig. 4(a), several representative original trajectories of PEPT tracers are depicted alongside their corresponding deterministic sub-trajectories, in this case at the fourth level of decomposition (L), exemplifying the smooth movement of tracers that represents flow motion at the largest scale. The selection of the right number of decomposition levels to be used will be discussed in Sec. IV A 2. From such trajectories, the Lagrangian instantaneous and mean PEPT velocities are estimated based, respectively, on the original and deterministic trajectories. Contour maps of the instantaneous and deterministic axial velocities normalized with respect to the mean velocity (U_b) are presented in Fig. 4(b), while the corresponding radial velocity profiles are plotted in Fig. 4(c). The contour maps reveal that the instantaneous and deterministic axial velocity distributions are largely similar, although some heterogeneity is observed in the contour map of the mean velocity. Comparing the radial profiles of axial velocity in Fig. 4(c), the mean (deterministic) profile is smaller than the instantaneous profile, particularly in the central region of the pipe, the difference being equal to the fluctuation velocity. Additionally, the deterministic profile exhibits a maximum bulk (background) velocity along the centerline, indicating that the predominantly large-scale fluid movement occurs in the core region of the pipe.

2. Fluctuating velocity statistics

Thy only input parameter required for this proposed multiscale methodology is the number of decomposition levels to be adopted, i.e., L in Eq. (5). There is no universal approach for selecting an appropriate decomposition level, which depends on the process at hand and the specific purpose of the analysis. Considering Eq. (6), the higher the level of decomposition of a time series, the more sub-signals and detailed information is captured which increases the contribution of the fluctuating part of the instantaneous velocity compared to that of the mean velocity. Too high or too low a decomposition level would lead to erroneous results. Therefore, the optimum decomposition level will strike the right balance between these two velocity components, giving the most accurate estimate of the instantaneous velocity. Here, we used turbulence intensity data from DNS simulations available in the literature as a benchmark to inform the selection of a suitable decomposition level; the mean velocity profiles yielded by the DNS simulations were validated by LDA measurements.[22]

The fluctuating velocity components derived from decomposed PEPT Lagrangian trajectories at different L values were, therefore, compared with those obtained from the DNS simulations. The local Lagrangian fluctuating velocity components at different decomposition levels were obtained from Eq. (6) and treated in a manner similar to the mean and instantaneous velocities, enabling the construction of radial profile plots of turbulent intensities. The root mean square (rms) of PEPT fluctuating velocities at different L values, normalized by the mean velocity, in the radial, azimuthal, and axial directions are presented in Fig. 5, alongside those obtained from DNS simulations available at $Re = 7500$, which is only slightly lower than $Re = 7800$ at which the PEPT measurements were obtained. There is optimal agreement between the fluctuating velocity components from PEPT and DNS at a decomposition level $L = 4$.

Using $L = 4$, the values of turbulent kinetic energy based on PEPT measurements were calculated using Eq. (8) and are depicted in

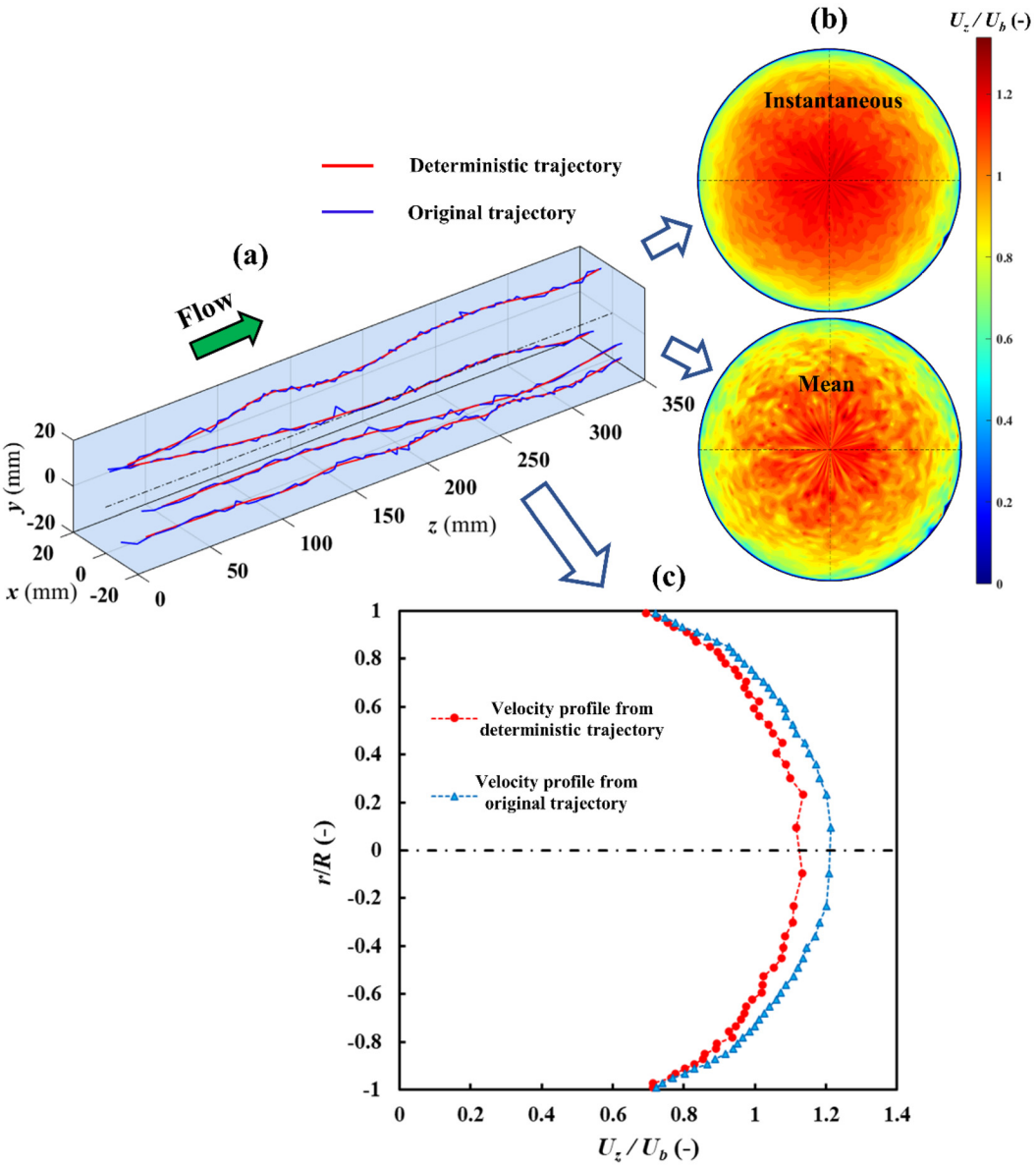

FIG. 4. Illustration of (a) typical 3D original and deterministic PEPT trajectories, (b) contour maps of instantaneous and deterministic axial velocities, and (c) radial profiles of instantaneous and deterministic axial velocities.

Fig. 6 in the form of normalized radial distributions across the pipe. There is a symmetrical bimodal distribution of TKE values characterized by two peaks situated near the pipe wall. The low TKE region observed in the center of the pipe corresponds to a region with relatively low turbulence, where the dominant flow motion is governed by large-scale movements. Turbulence intensity increases away from the center toward the pipe wall up to $r \approx 0.90\,R$, where it drops sharply to zero. Thus, it appears that the region away from the center contributes a higher proportion of small-scale movements. This result suggests that injection of material in this region would be more effective for mixing.

B. Particle-liquid flow

The introduction of coarse particles into a liquid flow within a pipe can have a substantial impact on the turbulent characteristics of the flow. The particles act as obstacles that disrupt fluid motion, thereby altering turbulence properties including turbulent kinetic energy. The interaction between particles and turbulent eddies gives rise to a complex interplay involving momentum transfer and energy dissipation. In Secs. IV B 1–3, the multiscale analysis of 3D Lagrangian trajectories developed here is used to explore the influence of introducing coarse particles of various sizes and densities at

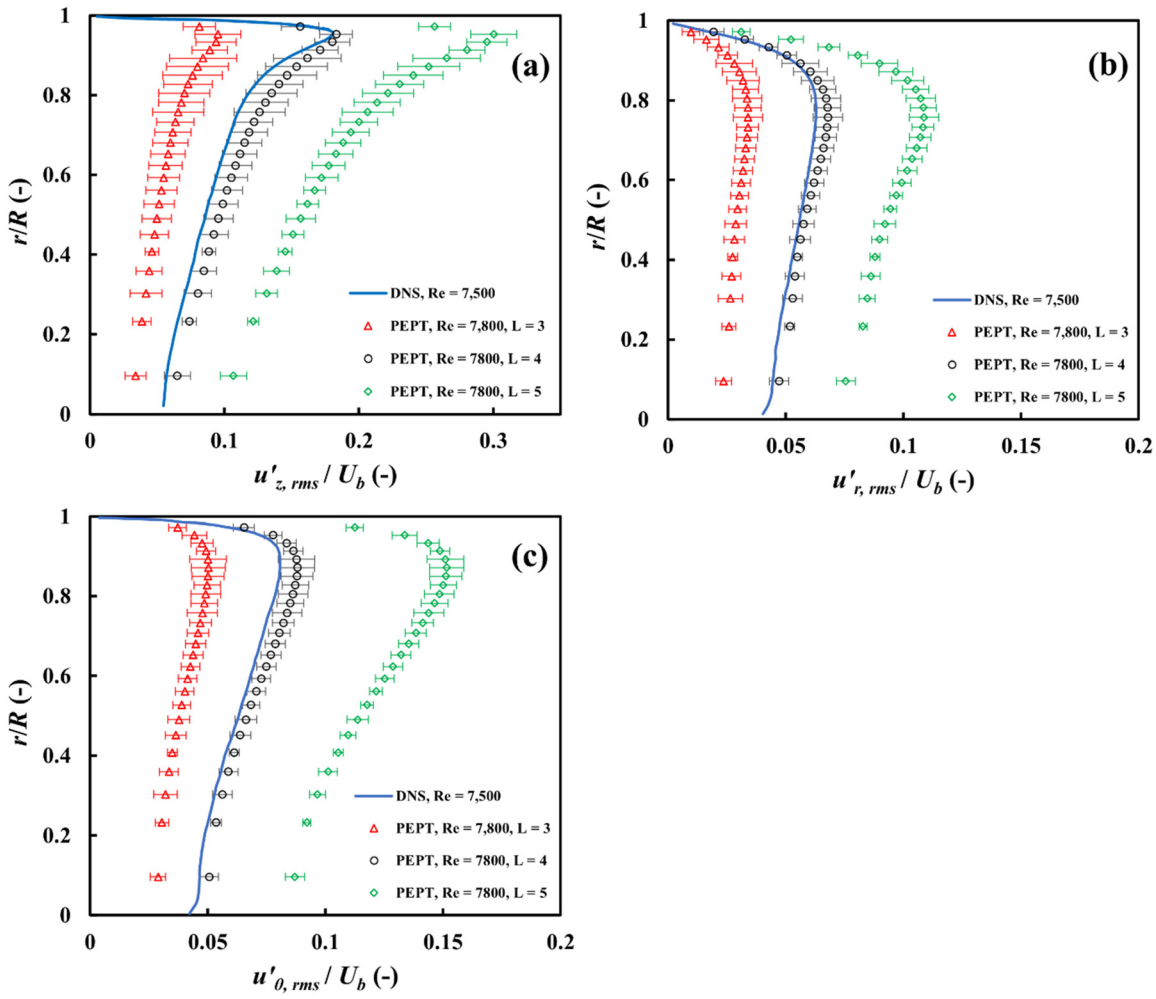

FIG. 5. Normalized turbulence intensities in (a) axial, (b) radial, and (c) azimuthal directions: PEPT measurements at different decomposition levels compared to DNS simulations.

various concentrations (Table I) on the TKE profiles within the sugar solution flow described above.

1. Effects of particle concentration

The radial TKE profiles of the carrier fluid conveying nearly neutrally buoyant particles of $d_p = 4$ mm and $\rho_r = 1.02$ at different solid loadings from 6 to 30 vol. % are depicted in Fig. 7 along with the corresponding radial particle concentration profiles. With the addition of 6 vol. % solid particles, a reduction in local TKE values is observed compared to the single-phase flow, notably in the lower half of the pipe section where the local particle concentration is greater than the mean concentration. However, as more solid particles are added, the local TKE values increase and the whole profile shifts to the right. There is a considerable jump in TKE when C_s increases from 6 to 12 vol. %, but the increment gradually reduces at higher particle concentrations becoming almost negligible from 21 to 31 vol. %, suggesting the existence of a TKE plateau at higher solid loadings. These results indicate that the introduction of coarse particles into a single-phase flow has two counteracting effects: (i) the TKE of the carrier fluid tends to decrease due to energy transfer to the particles, resulting in a dampening effect on turbulence intensity; and (ii) concurrently, particles generate additional eddies in the flow through particle–fluid and particle–particle interactions, leading to increased fluid fluctuations. At low solid loadings, the TKE attenuation effect dominates, while TKE amplification becomes more pronounced with increased particle concentrations due to enhanced particle–fluid and particle–particle interactions, tending toward a plateau beyond which further particle addition has little effect.

2. Effects of particle size

The radial profiles of fluid TKE in a particle-liquid flow of nearly neutrally buoyant particles of various sizes at a mean solid concentration of 21 vol. % are presented in Fig. 8 alongside the corresponding radial particle concentration profiles. The results show that the

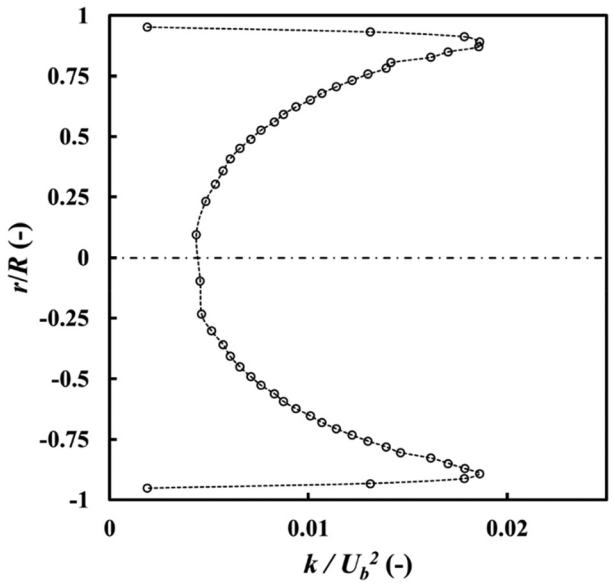

FIG. 6. Radial distribution of normalized turbulent kinetic energy estimated from PEPT measurements: single-phase flow; $Re = 7800$.

introduction of larger particles leads to increased turbulence intensity in the carrier fluid. Furthermore, turbulence amplification is more pronounced when increasing the particle size from 4 to 6 mm compared to the increase from 2 to 4 mm. It appears, thus, that larger particles generate stronger eddies that result in more heightened fluctuations in the carrier fluid. The remarkable axial symmetry of the TKE plots is due to the absence of significant skewness in the distribution of the solid phase across the pipe [Fig. 8(b)].

3. Effects of particle density

The impact of particle density on the fluid TKE profiles is illustrated in Fig. 9, where the TKE plots are shown for particle density ratios of 1.02 and 1.14. For a given particle size, denser particles cause more fluid turbulence than lighter ones. Denser particles exhibit stronger interactions with the surrounding liquid compared to lighter particles due to their greater inertia and momentum, leading to increased momentum exchange and energy dissipation within the flow. Denser particles moving through the liquid induce disturbances in the flow, resulting in velocity fluctuations and the formation of vortices. These disturbances act as sources of turbulent kinetic energy, thereby contributing to an increase in the overall turbulence intensity. The stronger particle–fluid interactions and enhanced mixing facilitate the transfer of energy across different length scales within the flow, further amplifying turbulence intensity. The near axial symmetry of the TKE plots is driven by the nearly symmetrical solid distribution plots shown in Fig. 9(b).

V. CONCLUSION

An experimental–theoretical methodology has been developed to investigate the characteristics of turbulence in horizontal single-phase and particle-liquid pipe flows. By utilizing 3D Lagrangian trajectories of the carrier fluid obtained through a technique of positron emission

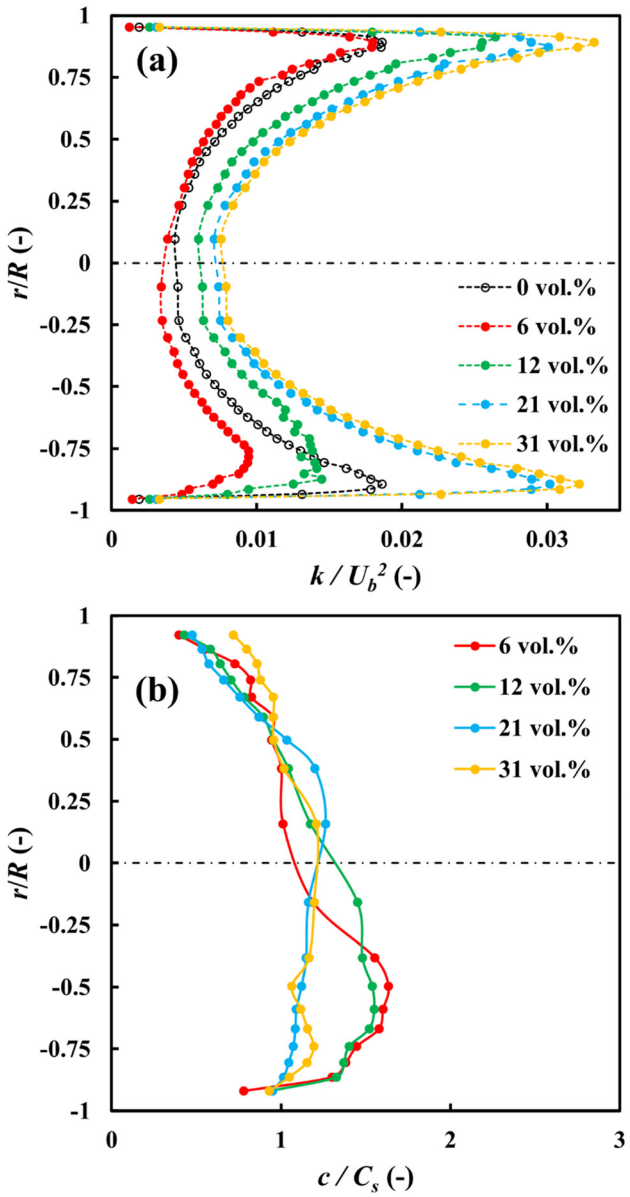

FIG. 7. Radial distributions of (a) fluid turbulent kinetic energy and (b) particle concentration for different solid loadings: $d_p = 4$ mm, $\rho_r = 1.02$.

particle tracking and applying a discrete wavelet transform, the local fluctuating velocity components and turbulent kinetic energy profiles were analyzed at different scales. The accuracy of the PEPT measurements was validated for the single-phase flow by CFD simulation and the well-known one-seventh power law relationship for the turbulent pipe flow. Direct numerical simulations (DNS) data were used as a benchmark to fine-tune the wavelet analysis before being applied to the investigation of more complex particle-liquid flows.

In particle-liquid flows, the results demonstrated that the particle size and density have significant effects on liquid turbulence. The

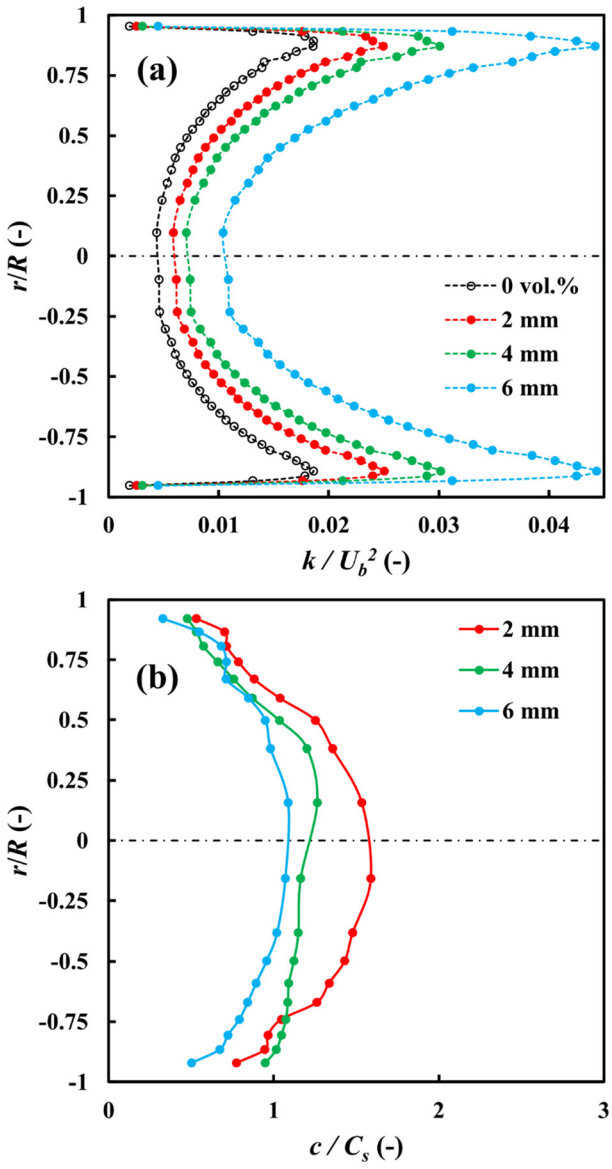

FIG. 8. Radial distributions of (a) fluid turbulent kinetic energy and (b) particle concentration for different particle sizes: $C_s = 21$ vol. %, $\rho_r = 1.02$.

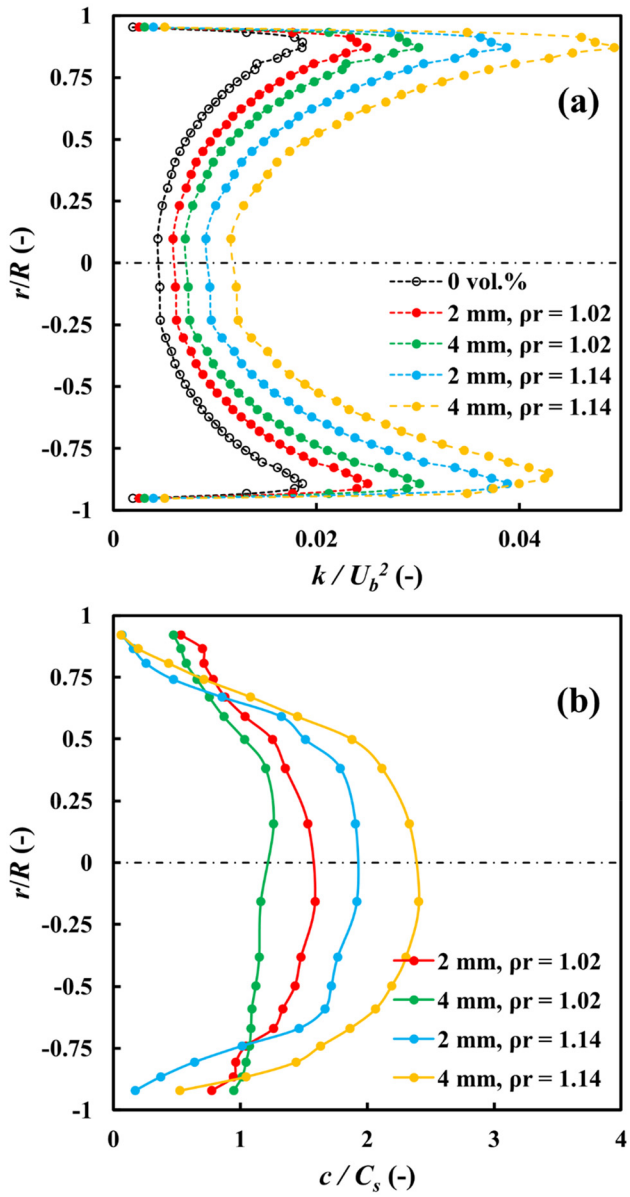

FIG. 9. Radial distributions of (a) fluid turbulent kinetic energy and (b) particle concentration for different particle to fluid density ratios: $C_s = 21$ vol. %.

introduction of larger and denser particles led to higher turbulence intensities in the carrier fluid. Denser and larger particles exhibited a more pronounced interaction with the surrounding liquid, resulting in increased momentum exchange and energy dissipation within the flow. These interactions introduced additional sources of turbulence generation and dissipation, leading to enhanced fluctuations. Low particle concentrations lead to reduced turbulence while higher concentrations enhance turbulence up to a point beyond which further increases have a negligible effect on turbulence intensity. The findings of this study provide valuable insight into the dynamics of particle-liquid pipe flows potentially aiding the rational design of industrial flows across a spectrum of applications.

ACKNOWLEDGMENTS

This work was supported by EPSRC Programme Grant EP/R045046/1: Probing Multiscale Complex Multiphase Flows with Positrons for Engineering and Biomedical Applications (PI: Professor M. Barigou, University of Birmingham).

AUTHOR DECLARATIONS

Conflict of Interest

The authors have no conflicts to disclose.

Author Contributions

Chiya Savari: Conceptualization (equal); Formal analysis (lead); Investigation (lead); Methodology (equal); Validation (equal); Visualization (lead); Writing – original draft (lead). **Mostafa Barigou:** Conceptualization (equal); Funding acquisition (lead); Methodology (equal); Project administration (lead); Resources (lead); Supervision (lead); Validation (equal); Writing – review & editing (lead).

DATA AVAILABILITY

The data that support the findings of this study are available within the article.

NOMENCLATURE

Symbols

A_j	Approximate sub-signal at jth level
C_s	Volumetric mean solid concentration (vol. %)
c	Local particle concentration
D_j	Detail sub-signal at jth level
d_p	Particle diameter (m)
d_t	Tracer diameter (m)
$\boldsymbol{e}_x$, $\boldsymbol{e}_y$, $\boldsymbol{e}_z$	Unit vectors in x, y, and z direction
k	Turbulent kinetic energy ($m^2\ s^{-2}$)
L	Number of decomposition levels
n	Number of data points
r	Radial position (m)
R	Pipe radius (m)
Re	Pipe Reynolds number
St	Stokes number
T	3D Lagrangian trajectory
t	Time (s)
u	Instantaneous velocity ($m\ s^{-1}$)
$\overline{u}$	Mean velocity ($m\ s^{-1}$)
u'	Fluctuation velocity ($m\ s^{-1}$)
U_b	Mean flow velocity ($m\ s^{-1}$)
U_z	Mean axial velocity ($m\ s^{-1}$)
x	x-direction position (m)
x_{det}, y_{det}, z_{det}	x-, y-, and z-direction deterministic Lagrangian displacement (m)
x_{sto}, y_{sto}, z_{sto}	x-, y-, and z-direction stochastic Lagrangian displacement (m)
y	y-direction position (m)
z	z-direction position (m)

Greek Symbols

υ	Kinematic viscosity ($m^2\ s^{-1}$)
μ	Viscosity ($kg\ m^{-1}\ s^{-1}$)
ρ	Liquid density ($kg\ m^{-3}$)
ρ_r	Particle to liquid density ratio
ρ_t	Tracer particle density ($kg\ m^{-3}$)
ψ	Wavelet mother function

Abbreviations

CFD	Computational fluid dynamics
DNS	Direct numerical simulation
DWT	Discrete wavelet transform
LDA	Laser Doppler anemometry
PEPT	Positron emission particle tracking
PIV	Particle image velocimetry
TKE	Turbulent kinetic energy

REFERENCES

[1]S. Mishra, H. Chandra, and A. Arora, "Solid liquid non-Newtonian fluid flow in pipe: A review," Acta Mech. Slov. **16**, 62 (2012).
[2]E. Rabinovich and H. Kalman, "Threshold velocities of particle-fluid flows in horizontal pipes and ducts: Literature review," Rev. Chem. Eng. **27**, 215 (2011).
[3]C. G. Lomas, *Fundamentals of Hot Wire Anemometry* (Cambridge University Press, 2011).
[4]A. Kalpakli Vester, S. S. Sattarzadeh, and R. Örlü, "Combined hot-wire and PIV measurements of a swirling turbulent flow at the exit of a 90° pipe bend," J. Visualization **19**, 261 (2016).
[5]F. Durst, R. Müller, and J. Jovanovic, "Determination of the measuring position in laser-Doppler anemometry," Exp. Fluids **6**, 105 (2004).
[6]J. M. Wallace and P. V. Vukoslavčević, "Measurement of the velocity gradient tensor in turbulent flows," Annu. Rev. Fluid Mech. **42**, 157 (2010).
[7]G. Wang, F. Yang, K. Wu, Y. Ma, C. Peng, T. Liu, and L.-P. Wang, "Estimation of the dissipation rate of turbulent kinetic energy: A review," Chem. Eng. Sci. **229**, 116133 (2021).
[8]A. Al-Homoud and M. Hondzo, "Energy dissipation estimates in oscillating grid setup: LDV and PIV measurements," Environ. Fluid Mech. **7**, 143 (2007).
[9]P. Saarenrinne and M. Piirto, "Turbulent kinetic energy dissipation rate estimation from PIV velocity vector fields," Exp. Fluids **29**, S300 (2000).
[10]A. Delafosse, M.-L. Collignon, M. Crine, and D. Toye, "Estimation of the turbulent kinetic energy dissipation rate from 2D-PIV measurements in a vessel stirred by an axial Mixel TTP impeller," Chem. Eng. Sci. **66**, 1728 (2011).
[11]M. Barigou, "Particle tracking in opaque mixing systems: An overview of the capabilities of PET and PEPT," Chem. Eng. Res. Des. **82**, 1258 (2004).
[12]C. Savari, H. A. Sheikh, and M. Barigou, "Lagrangian recurrence tracking: A Novel approach for description of mixing in liquid and particle–liquid flows," Ind. Eng. Chem. Res. **60**, 18501 (2021).
[13]H. A. Sheikh, C. Savari, and M. Barigou, "Lagrangian stochastic modelling of liquid flow in a mechanically agitated vessel," Chem. Eng. Sci. **249**, 117318 (2022).
[14]K. Li, C. Savari, and M. Barigou, "Computation of Lagrangian coherent structures from experimental fluid trajectory measurements in a mechanically agitated vessel," Chem. Eng. Sci. **254**, 117598 (2022).
[15]Z. Yang, C. Savari, and M. Barigou, "Numerical and experimental investigations of horizontal turbulent particle–liquid pipe flow," Ind. Eng. Chem. Res. **61**, 12040 (2022).
[16]H. A. Sheikh, C. Savari, and M. Barigou, "A data-driven stochastic model for velocity field and phase distribution in stirred particle-liquid suspensions," Powder Technol. **411**, 117940 (2022).
[17]S. C. Bailey, M. Hultmark, J. Schumacher, V. Yakhot, and A. J. Smits, "Measurement of local dissipation scales in turbulent pipe flow," Phys. Rev. Lett. **103**, 014502 (2009).
[18]G. L. Eyink, "Turbulent flow in pipes and channels as cross-stream "inverse cascades" of vorticity," Phys. Fluids **20**, 125101 (2008).
[19]M. J. Shensa, "The discrete wavelet transform: Wedding the a Trous and Mallat algorithms," IEEE Trans. Signal Process. **40**, 2464 (1992).
[20]D. Sundararajan, *Discrete Wavelet Transform: A Signal Processing Approach* (John Wiley & Sons, 2016).
[21]A. M. Dehkordi and C. Savari, "Effects of contaminants on the mass-transfer characteristics of a two-impinging-streams gas-liquid reactor," Chem. Eng. Technol. **34**, 1797 (2011).
[22]C. Wagner, T. Hüttl, and R. Friedrich, "Low-Reynolds-number effects derived from direct numerical simulations of turbulent pipe flow," Comput. Fluids **30**, 581 (2001).
[23]H. Saffari, R. Moosavi, N. M. Nouri, and C.-X. Lin, "Prediction of hydrodynamic entrance length for single and two-phase flow in helical coils," Chem. Eng. Process. **86**, 9–21 (2014).

[24]P. Fairhurst, M. Barigou, P. Fryer, J. Pain, and D. Parker, "Using positron emission particle tracking (PEPT) to study nearly neutrally buoyant particles in high solid fraction pipe flow," Int. J. Multiphase Flow **27**, 1881 (2001).
[25]P. Pianko-Oprych, A. Nienow, and M. Barigou, "Positron emission particle tracking (PEPT) compared to particle image velocimetry (PIV) for studying the flow generated by a pitched-blade turbine in single phase and multi-phase systems," Chem. Eng. Sci. **64**, 4955 (2009).
[26]C. Savari, K. Li, and M. Barigou, "Multiscale wavelet analysis of 3D Lagrangian trajectories in a mechanically agitated vessel," Chem. Eng. Sci. **260**, 117844 (2022).
[27]C. Savari and M. Barigou, "Lagrangian wavelet analysis of turbulence modulation in particle–liquid mixing flows," Phys. Fluids **34**, 115121 (2022).
[28]K. Li, C. Savari, H. A. Sheikh, and M. Barigou, "A data-driven machine learning framework for modeling of turbulent mixing flows," Phys. Fluids **35**, 015150 (2023).
[29]X. Lian, C. Savari, K. Li, and M. Barigou, "Coupled smoothed particle hydrodynamics and discrete element method for simulating coarse food particles in a non-Newtonian conveying fluid," Phys. Fluids **35**, 043325 (2023).
[30]K. Li, C. Savari, and M. Barigou, "Predicting complex multicomponent particle–liquid flow in a mechanically agitated vessel via machine learning," Phys. Fluids **35**, 053301 (2023).
[31]S. Bakalis, P. Fryer, and D. Parker, "Measuring velocity distributions of viscous fluids using positron emission particle tracking (PEPT)," AIChE J. **50**, 1606 (2004).
[32]F. Lucci, A. Ferrante, and S. Elghobashi, "Is Stokes number an appropriate indicator for turbulence modulation by particles of Taylor-length-scale size?" Phys. Fluids **23**, 025101 (2011).
[33]A. Guida, A. W. Nienow, and M. Barigou, "PEPT measurements of solid–liquid flow field and spatial phase distribution in concentrated monodisperse stirred suspensions," Chem. Eng. Sci. **65**, 1905 (2010).
[34]H. L. Resnikoff, R. O. Wells, H. L. Resnikoff, and R. O. Wells, "The Mallat algorithm," in *Wavelet Analysis: The Scalable Structure of Information* (Springer, 1998), pp. 191–201.
[35]L. J. De Chant, "The venerable 1/7th power law turbulent velocity profile: A classical nonlinear boundary value problem solution and its relationship to stochastic processes," Appl. Math. Comput. **161**, 463 (2005).